Experimental investigation on the optimal injection and combustion phasing for a direct injection hydrogen-fuelled internal combustion engine for heavy-duty applications

International Journal of Hydrogen Energy 100 (2025) 398–406

Contents lists available at ScienceDirect

International Journal of Hydrogen Energy

journal homepage: www.elsevier.com/locate/he

Experimental investigation on the optimal injection and combustion phasing for a direct injection hydrogen-fuelled internal combustion engine for heavy-duty applications

Andrea Piano [a,*], Francesco Pucillo [a], Federico Millo [a], Sergio Giordana [b], Nicola Rapetto [b], Christoph Schuette [c]

[a] Politecnico di Torino, Energy Department, Italy
[b] FPT Industrial S.p.A, Italy
[c] FPT Motorenforschung AG, Switzerland

ARTICLE INFO

Handling Editor: Dr M Djukic

Keywords:
Hydrogen
Internal combustion engines
Direct injection
Hydrogen combustion

ABSTRACT

In the current context of increasing demand for clean transportation, hydrogen usage in internal combustion engines (ICEs) represents a viable solution to abate all engine-out criteria pollutants and almost zeroing CO_2 tailpipe emissions. Indeed, the wider flammability limits thanks to the higher flame propagation speed and the lower minimum ignition energy compared with conventional fuels, extend the stable combustion regime to leaner mixtures thus allowing high thermal efficiency keeping under control the NO_X emissions. To fully exploit the potential of hydrogen as a fuel and to avoid undesired abnormal combustion processes, a deep characterization of the combustion process is needed. With this aim, a 6-cylinder, 12.9-L heavy-duty engine was converted from a port-fuel injected compressed natural gas to a direct injected hydrogen spark ignition one. A wide experimental campaign was carried out, consisting of several sweeps of relative air-fuel ratios, spark advances, and injection timings at different engine speeds and loads, aiming to define a preliminary engine map. The effect of each calibration parameter at different engine load and speed has been analyzed through the combination of relevant combustion parameters, as well as NO_X emissions. The results have demonstrated the critical influence of the mixture inhomogeneity when the injection is retarded through the top dead center firing, as indicated by the increase in NO_X emissions and combustion variability. The analysis of the combustion timing has indicated the dependence of the optimal MFB50 on the relative air-fuel ratio. Lastly, the analysis of 200 consecutive cycles for each operating condition has allowed the evaluation of the influence of the main calibration parameters on the cyclic variability, thus providing further insights about the lean limit of hydrogen in ICE.

1. Introduction

In the current context of growing efforts to mitigate the effects of climate change [1,2], the transport sector is facing significant challenges due to the need to transition away from fossil fuel-based powertrains. In the next years, the transport demand is expected to grow according to various estimates [3], while the regulatory framework will simultaneously require a significant reduction of CO_2 emissions [1]. For these reasons, the industry is exploring several innovative technological solutions to meet these regulatory requirements. This process involves the inherent difficulty of balancing the technical feasibility with the economic and social sustainability, as well as customer acceptance. Therefore, solutions that preserve existing manufacturing processes and supply chains are preferred to exploit potential synergies during the transition phase. In this context, clean hydrogen, produced from renewable energy sources, is expected to play a significant role in the transition towards a zero-carbon economy, particularly in the hard-to-abate energy sector, including long-haul transport. Over the past few years, the usage of hydrogen for transport has regained interest [4], also driven by the favorable legislative framework, as evidenced by the hydrogen strategies set by most of the developed countries worldwide [5–7]. In many transport-related applications, there is noticeable interest in using hydrogen in fuel cell systems. However, the high-load demand and the requirement in terms of hydrogen purity [8] make

* Corresponding author.
E-mail address: andrea.piano@polito.it (A. Piano).

https://doi.org/10.1016/j.ijhydene.2024.12.194
Received 16 September 2024; Received in revised form 26 November 2024; Accepted 10 December 2024
Available online 24 December 2024

the usage of hydrogen as fuel in internal combustion engines (ICEs) a robust alternative. Furthermore, the favorable combustion properties of hydrogen (e.g., high laminar flame speed over a wide range of air-to-fuel ratios) can result in high thermodynamic efficiency with a reduced knock risk [9]. Another advantage of using hydrogen as fuel in ICEs is the significant reduction of engine-out pollutant emissions and the abatement of CO_2 emissions. Indeed, a significant reduction of NO_X emissions can be achieved through the exploitation of a lean combustion approach, which is beneficial also for efficiency improvement [10].

Initial explorations of the hydrogen's potential in ICEs were conducted by adopting a port fuel injection (PFI) system [11]. This choice has been mainly driven by the easier conversion of existing engines, thus the shorter time-to-market [12–14]. The main advantage of this solution is the less complex control strategy, and the almost perfect homogenization of the mixture [15]. The potential is, however, constrained by the low density of hydrogen, which affects the volumetric efficiency and consequently the power output [14]. In addition, PFI configurations have been demonstrated to be prone to backfire [16,17], a pre-ignition of the fuel during the intake stroke that directs combustion through the intake manifold. A different approach relies on the direct injection (DI) of the hydrogen that has shown significant potential to overcome the abovementioned limitations. Firstly, the risk of backfire can be considered negligible when the fuel is injected during the compression stroke; secondly, the volumetric efficiency is not negatively affected by the fuel injection thus increasing the achievable power output. Indeed, mainly for gaseous fuels, the low density plays a role in affecting the compression work. Due to its density (0.09 kg/m3 at 1 bar, 20 °C), hydrogen occupies about 30% of the volume of the whole mixture at stoichiometric conditions. Consequently, the compression work tends to increase with advanced injections [18]. However, DI configuration is characterized by higher complexity since the control strategy has to face the challenge of an adequate homogenization of the air-fuel mixture. As evidenced in Matthias et al. [19], this aspect is crucial for a regular combustion process and to limit NO_X emissions. To increase the time available for the mixture formation and improve the homogeneity of the mixture, high injection pressures can be exploited, thus shortening the injection event. However, the injection pressure needs to be limited to guarantee an adequate vehicle range. Therefore, the optimal injection timing should be sufficiently advanced to guarantee enough time to homogenize the mixture, but also retarded as much as possible to reduce the compression work and the hydrogen backflow through the intake ports. Hydrogen presents a high laminar flame speed over a broad range of λ values. Thus, the exploitation of lean combustion can guarantee increased efficiency, due to the reduction of heat exchange losses without significant drawbacks on combustion efficiency. Consequently, the optimization of combustion timing has to consider the impact on combustion stability and NO_X emission at different λ values. Moreover, knock occurrence limits the achievable combustion advance, despite a higher knock resistance compared to conventional fuels has been reported by several works [20,21]. Additional challenges have to be addressed when adopting a DI system. For instance, in the case of jet-wall interaction, the lubricant film could be diluted and absorbed within the mixture, thereby leading to higher PM emissions [22] or acting as a pre-ignition source. This latter can be also induced by the presence of rich local pockets due to poor air-hydrogen mixing, as highlighted by Grabner et al. [23]. In this context, low-pressure direct-injection systems result as the best compromise among costs, range, system complexity, and power output. Therefore, high interest is devoted to this solution with a special focus in the heavy-duty sector, as demonstrated by the studies of [9,24,25].

In this paper, a 6-cylinder, 12.9-L heavy-duty engine was selected as a case study. The engine was converted from a PFI compressed natural gas (NG) engine to a DI hydrogen spark ignition one. The goal was mainly oriented to limit the complexity of the conversion, thus exploiting the hydrogen potential without modifying the base engine characteristics. With this aim, a wide experimental campaign was carried out, evaluating the impact of the different calibration parameters, such as the relative air-fuel equivalence ratio (λ), spark advance, and injection timing, on the engine performance. More in detail, the analysis investigated brake efficiency, combustion variability and NO_X emissions formation at different engine operating conditions. Despite particle emissions have been recognized as an important factor in DI H_2 ICEs [22], it was not investigated in this analysis, since it was not considered as a limiting factor. Indeed, particle formation from oil dilution does not show a clear dependency on ignition timing or injection timing [26], especially when a dedicated spay cap is adopted to avoid spray-wall interaction as in the present study, and tailored aftertreatment systems have demonstrated high efficacy in ensuring compliance with regulatory standards [27,28]. First of all, the effect of injection timing was investigated to define the optimal injection window that maximizes the efficiency limiting the hydrogen stratification and thus the NO_X emissions. A systematic understanding of how mixture inhomogeneity contributes to combustion variability is still lacking. Then, the effect of the combustion phasing was analyzed, highlighting its impact on the cycle-by-cycle variability. The outcomes of this analysis have been then used for the definition of a preliminary engine map.

2. Experimental setup

The experimental investigation was performed on a 12.9-L heavy-duty 6-cylinder engine. The engine was derived from a current production PFI NG engine. To allow hydrogen operations, some modifications were made.

- Combustion system: the piston bowl design was modified to enhance the air-fuel mixing, while the original flat head was kept unchanged. In Fig. 1, the two different piston bowls are presented. Compared to the baseline bowl, the adopted piston bowl presents a wider lens design. Thanks to the interaction of the fuel jet with the piston bowl, a tumble motion able to enhance air-fuel mixing is induced. A top view of the cylinder head is reported in Fig. 2. The spark plug, properly designed for hydrogen operation, was maintained in the central position in the cylinder head, while the hydrogen injector was located in a lateral position. The outwardly – opening injector operates with a maximum injection pressure equal to 40 bar, employing a strategy based on a single-injection event. A 1-hole dedicated spray guiding cap was designed with the aim of enhancing the mixing rate between the hydrogen jet and the surrounding air. Although the 1-hole design does not provide the same improvement of the mixing rate compared to multi-hole injector caps [15,29], it was selected for the easier manufacturing process, and for the reduced risk of insufficient scavenging of the cap which can act as a potential source of pre-ignition [30,31]. The compression ratio of the NG engine was reduced from 12 to 11 to reduce the auto-ignition tendency.

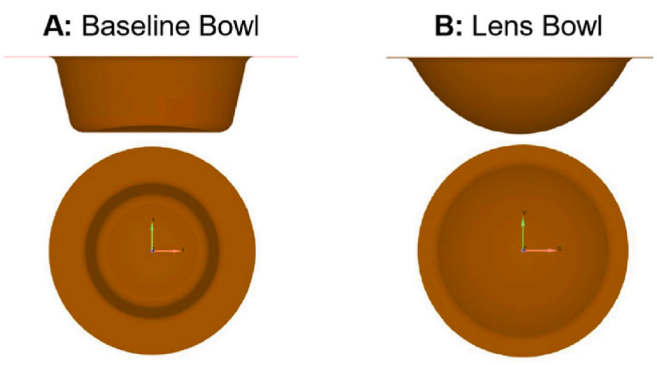

Fig. 1. Comparison of the piston bowl design. A: baseline, from NG engine; B: lens design adopted after the retrofitting.

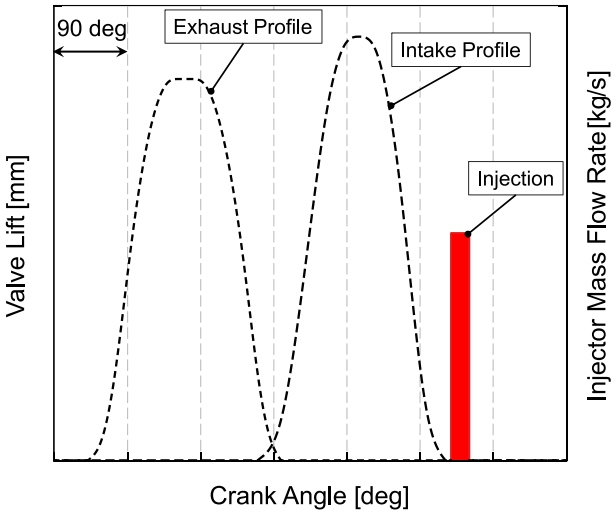

Fig. 2. Top view of the cylinder head.

- Camshaft: the intake camshaft was modified to have a wider profile compared to the baseline NG one since the goal was to exploit lean operation with hydrogen. In addition, the profile was optimized to prevent hydrogen backflow. Valve profiles and injection timing, for a specific operating condition, are presented in Fig. 3.
- Turbocharger: the requirement of high flow rates due to lean operation made necessary the exploitation of a variable geometry turbine (VNT).

The main features of the modified version of the engine are reported in Table 1.

2.1. Test matrix

Several operating conditions spread on the whole engine map were tested, ranging from 1100 to 2000 rpm and from 20% of maximum load to full load, as presented in Fig. 4.

For each engine operating condition, a series of sweeps was performed. First of all, the end of injection (EOI) was swept keeping the MFB50 (crank angle at which 50% of the fuel mass is burned) constant at 8 deg ATDCf and varying λ across three levels (i.e., 2.1, 2.5, 2.9). Minimum EOI (i.e., advanced injection event) was selected considering the injection event when the intake valves are still open; while the maximum value (i.e., retarded injection event) was fixed equal to −60 deg ATDCf to reduce the compression work due to the low density of hydrogen and at the same time to guarantee sufficient time for mixture homogenization. A further advance in injection event was not tested, due to the increased risk of fuel backflow through the intake manifold. At the same time, further retardation was not tested since the high backpressure at the injector outlet might affect the control of the

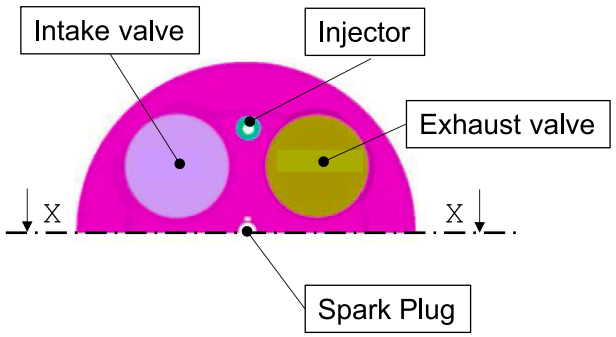

Fig. 3. Valve and injection timing diagram.

Table 1
Main characteristic of the engine under investigation.

Engine type	6 l L– DI TC H_2
Displacement	12.9 L
Bore x stroke	135 mm × 150 mm
Compression ratio	11:1
Bowl design	Lens
Turbocharger	VNT
Injection system	Low-pressure DI
Ignition	Prototype for H2

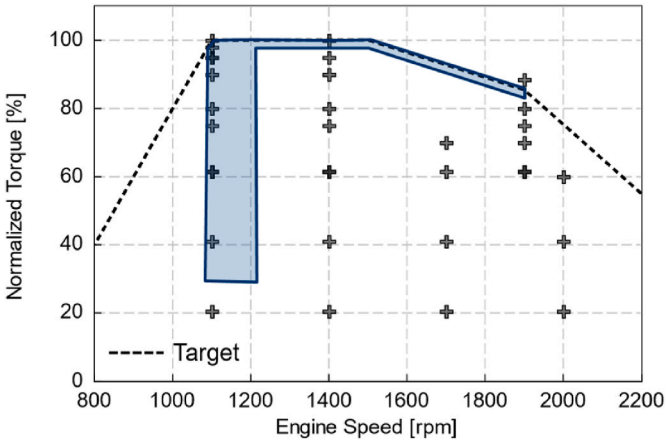

Fig. 4. Operating engine map. Crosses: tested engine operating conditions; Blue box: area of interest for long-haul applications. (For interpretation of the references to colour in this figure legend, the reader is referred to the Web version of this article.)

injected quantity. Then, a MFB50 sweep was performed at the three abovementioned λ levels but in this case the EOI was held constant and equal to −110 deg ATDCf, recognized as a value able to provide sufficiently homogeneous mixtures at different λ values. The most advanced spark timing was selected to have a sufficient margin on knock, while the most retarded one was defined where an increased number of very slow-burning cycles was verified. Moreover, further retard on combustion timing will cause unacceptable levels of combustion variability.

Fig. 5 shows the test matrix adopted in terms of EOI, λ, and MFB50 variations for each engine operating condition under investigation. 200 consecutive pressure cycles were acquired for each operating condition, thus allowing proper statistical analysis.

The target application of the engine under investigation is a class V 4x2 road tractor, which is typically employed for long-haul missions.

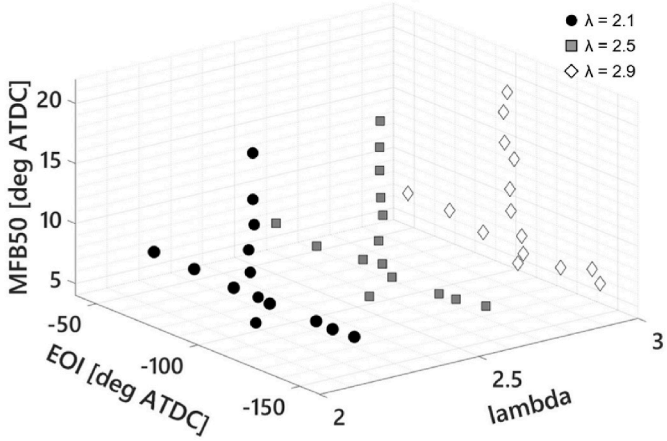

Fig. 5. EOI, MFB50 and λ variations for each engine operating condition.

Table 2
Experimental tests under investigation.

Test	Speed [rpm]	Load [%]	λ	MFB50 [deg ATDCf]	EOI [deg ATDCf]
#1 EOI sweep	1100; 2000	40; 60	2.1; 2.5; 2.9	8	−160 → −60
#2 MFB50 sweep	1100	40; 60	2.1; 2.5; 2.9	6 → 22	−110

The usual mission profile for this application, as derived from the pre-retrofitting engine map, is confined to the blue region zone highlighted in Fig. 4, located at around 1100 rpm from 30% to 100% of maximum load and at high load up to 1900 rpm. For this reason, in the present work, the operating point at 40% engine load at 1100 rpm has been selected, since it representative of a typical cruise point. Table 2 presents a summary of the experimental tests used for the present investigation.

3. Results and discussion

3.1. Test #1: EOI sweep – effect of injection timing under different λ conditions

The first test under investigation is the EOI sweep. As previously mentioned, having a perfect mixture homogeneity is a current challenge in hydrogen DI engines. One possible solution relies on advancing injection thus increasing the time available for mixing. However, due to the hydrogen density (0.09 kg/m^3 at 1 bar, 20 °C), the compression work increases when the injection is advanced, having a not negligible impact on the efficiency worsening. The exploitation of high injection pressure can also enhance the mixing rate and reduce the injection duration, but it is limited by the need to guarantee an adequate vehicle range. Therefore, the understanding of the impact of EOI on combustion, cyclic variability, and emissions formation phenomena is of paramount importance for the development of hydrogen-fuelled engines. For this reason, the impact of EOI variation for three different λ levels has been analyzed in terms of brake efficiency, coefficient of variation (CoV) of IMEP and NO_X emissions, as shown in Fig. 6. As abovementioned, during the test combustion anchor angle was kept constant and equal to 8 deg ATDCf.

Fig. 6 (A) shows the impact of the injection timing on the brake efficiency. Two distinct behaviors can be identified: advanced the injection timing (up to EOI = −140 deg ATDCf) does not affect the brake efficiency since hydrogen injection is performed when the intake valves are still open. Conversely, remarkable improvement in brake efficiency (~+1.5%) can be achieved with retarded injection as a result of the reduced compression work. This result is visible for each λ value tested. However, it is worth pointing out that the highest efficiency is achieved for λ = 2.5, in which the reduction of the heat exchange losses compensates for the longer combustion duration. As a reference, the efficiency achieved at this operating point exceeds the efficiency of the NG engine before the retrofitting by approximately 5%. Similar efficiency is obtained at λ = 2.9, except for the most retarded injection timing case, where the efficiency drops down. In this condition (EOI = −60 deg ATDCf), λ = 2.9 case shows also a sharp increase in IMEP variability (Fig. 6 (B)), highlighting a reduction of combustion stability mainly due to the progressive deterioration of the mixture homogeneity when the injection is retarded. However, this effect is visible only at the leanest mixture condition (i.e., λ = 2.9) where a lower jet penetration is expected [32], and thus a more difficult mixture homogenization, combined with a more diluted mixture which slows the flame propagation. The deterioration of the air-fuel mixture homogeneity when the injection is retarded is confirmed by NO_X emissions in Fig. 6 (C). The NO_X emissions trend is almost flat and constant except for the most retarded injection timing, at which a sharp rise is highlighted for all the λ tested. Given the well-known dependence of NO_X emissions on λ [10], this behavior can be linked to the fact that the flame reaches a local rich zone within the combustion chamber due to the lack of homogeneity, resulting in increased NO_X emissions. From a global point of view, the mixture enleanment leads to a NO_X reduction, as expected, while the EOI has a negligible impact on NO_X emissions formation except for the cases in which the inhomogeneity becomes relevant.

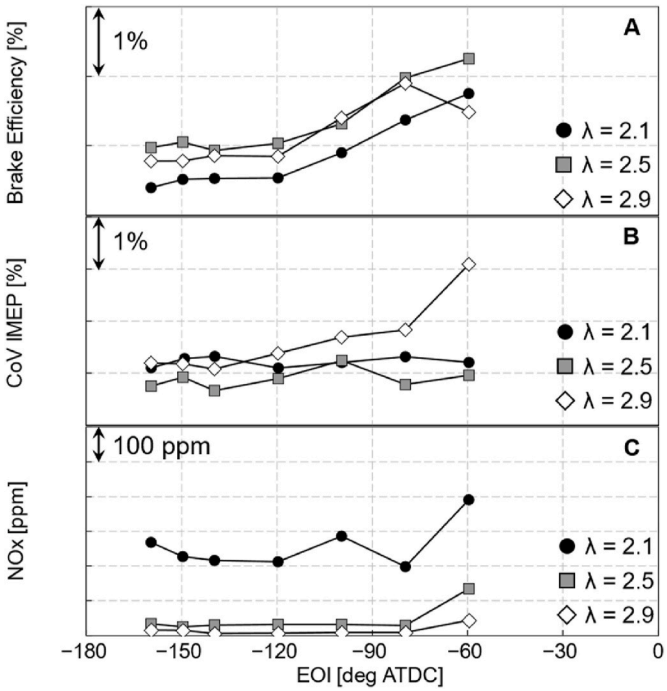

Fig. 6. Test #1 – EOI Sweep: effect of injection timing under different λ conditions.
A: Brake efficiency, B: CoV IMEP, C: NO_X emissions.

The EOI sweep has been performed also at a higher engine speed (2000 rpm) keeping constant the engine load. In this case, keeping constant the EOI, the time available for the mixing is reduced by a factor of 1.8 in comparison with the 1100 rpm. Fig. 7 shows the results in terms of CoV of IMEP and NO_X emissions for both the engine speeds at λ = 2.1, to focus the analysis on the mixing process effectiveness. From the NO_X

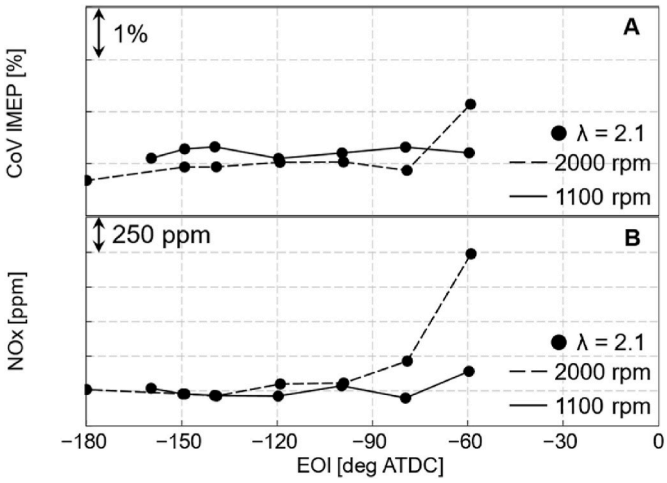

Fig. 7. Test #1 – EOI Sweep: effect of injection timing under different engine speeds.
A: CoV IMEP; B: NO_X emissions.

emissions (Fig. 7 (B)) it is evident that when the injection is retarded, the mixture becomes largely inhomogeneous for the 2000 rpm case: this latter, indeed, at EOI = −60 deg ATDCf shows an increase of around 900 ppm compared to the case at 1100 rpm. This homogeneity worsening at higher engine speeds is further confirmed by the IMEP variability (Fig. 7 (A)), in which an increase of 1% in the CoV of IMEP can be highlighted compared to the variability observed at 1100 rpm. A similar result was obtained by Li et al. [33], where the increase in engine speed led to a higher CoV of IMEP, as a result of a less homogeneous mixture.

To further investigate the combustion variability, the maximum of the in-cylinder pressure as a function of the duration of the early combustion phase (MFB0-10%) is plotted in Fig. 8. The correlation between combustion variability and the MFB0-10% was proposed by Matekunas [34]. In Fig. 8, each individual pressure cycle (i.e., 200) has been analyzed for each operating condition, sweeping the λ (2.1 in Fig. 8 (A); 2.5 in Fig. 8 (B); 2.9 in Fig. 8 (C)) and considering an early and a late injection phasing, in red and blue respectively. λ = 2.1 and λ = 2.5 cases show a clear trend: the individual cycles that exhibit longer early burn durations also present lower peak pressures, with an almost linear correlation as highlighted by the black dashed line, while the cycles at λ = 2.9 in Fig. 8 (C) show a more pronounced impact of the early burn duration. The peak pressure value is increased, mainly due to the increased boost pressure, while the burn duration is longer because of the reduced laminar flame speed. In addition, the late injection case shows several cycles with long MFB0-10% and reduced values of peak firing pressure corresponding to the peak pressure in motored conditions. These cases are characterized by slow flame propagation, by retarded MFB50, and thus reduced combustion efficiency. This behavior is also confirmed by the trend in IMEP variability depicted in Fig. 6 (B). Late injection is significantly more prone to the presence of slow-burning cycles due to the inhomogeneity in the proximity of the spark plug, where a laminar flame kernel starts to propagate after the spark discharge [35]. The relationship between the presence of several slow-burning cycles and the severe mixture inhomogeneity, characterized by leaner λ in the proximity of the spark plug, was verified in an optical investigation by Laichter et al. [36]. The results reported in Fig. 6 show agreement with respect to other studies. As expected, retarded injection provides a relevant benefit in brake efficiency: Liang [37] verified a brake efficiency increase of approximately 1.3% at 1600 rpm, 6 bar BMEP, λ = 2.5, while Schneider [24] verified around +1% in indicated efficiency at 1166 rpm, 10 bar BMEP, λ = 2.81. When the mixture inhomogeneity becomes more severe due to retarded injection timing, a notable increase in NO_X emissions is expected, as evidenced in Liang et al. [37]. Additionally, Kim [38] observed a sharp increase in combustion variability when the injection was performed at closed intake valves. Li [33] observed a comparable trend in combustion variability, with an increase of around 1.5% retarding the injection start after the intake valve closure. A similar increase in combustion variability was also verified at higher engine speed, which aligns with the trends shown in Fig. 7.

In Fig. 9, a comparison with the results obtained at 60% of maximum load at 1100 rpm is shown. For the sake of brevity, only the cases at λ = 2.1 and λ = 2.9 are reported. Retarding the injection timing provides similar advantages in brake efficiency (~+1.5%). A different behavior is present regarding λ. While at 40% of load the highest efficiency was achieved at the leaner λ, at 60% it was achieved at λ = 2.1. In this operating condition, the increase in the required boost pressure at λ = 2.9 leads to an increase of the pumping losses (PMEP), as effect of the higher turbine inlet pressure. This phenomenon, which is an indicator of an imperfect turbomatching, was analyzed in detail in Pucillo et al. [39]. The operating points at 60% of load does not show different trends in combustion variability compared to the lower load, as evident by Fig. 9 – (B). Fig. 9 – (C) highlights similar trends when injection timing is varied, while an increase in NO_X is verified at a higher load. This last behavior is well expected since higher temperatures are recognized to be a primary cause for NO_X formation.

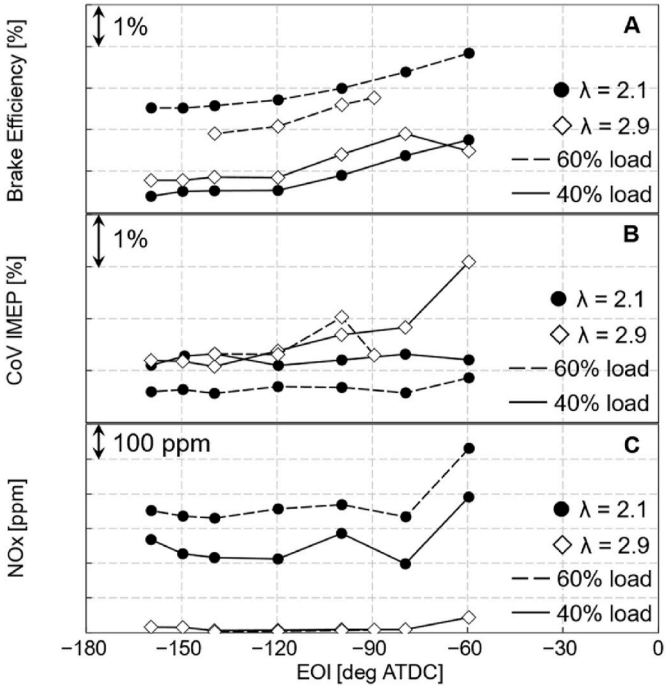

Fig. 9. Test #1 – EOI Sweep: effect of injection timing under different engine loads.
A: Brake Efficiency; B: CoV IMEP; C: NO_X emissions.

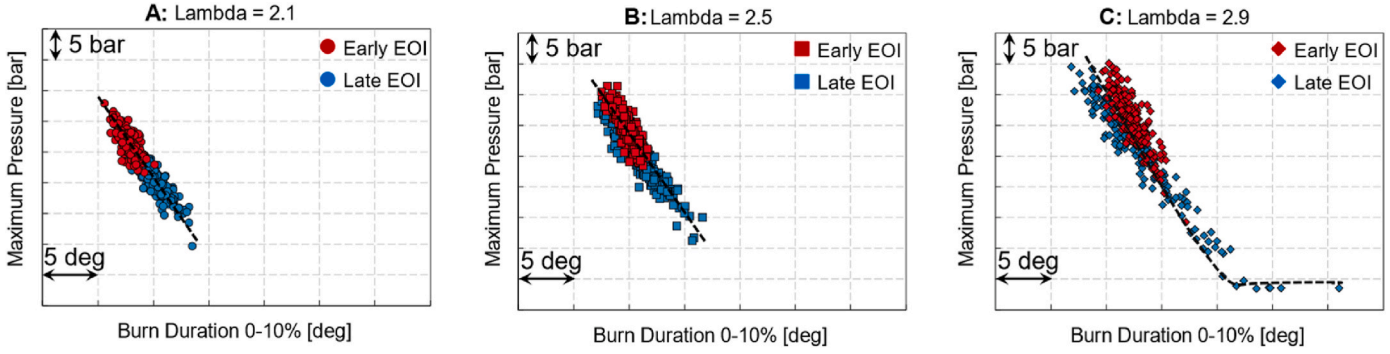

Fig. 8. Individual cycle analysis: maximum pressure as a function of MFB0-10%.
A: λ = 2.1; B: λ = 2.5; C: λ = 2.9.

3.2. Test #2: MFB50 sweep – effect of combustion timing under different λ conditions

As a second step of the analysis, a combustion phasing sweep has been performed for three different λ levels. Also in this case, the brake efficiency, the coefficient of variation (CoV) of IMEP, and the NO_X emissions have been analyzed and are depicted in Fig. 10 as a function of the MFB50 value, which has been adjusted by varying the spark timing. As mentioned in Table 2, the injection phasing has been kept constant and equal −110 deg ATDCf, to avoid the impact of the injection on the analysis and at the same time to guarantee enough time for the mixture homogenization.

As illustrated in Fig. 10 (A), at a constant combustion anchor angle the brake efficiency increases when the mixture becomes leaner, reaching its peak at λ = 2.9 for the most advanced combustion (i.e., MFB50 = 6 deg ATDCf). In this mixture condition, the efficiency loss due to combustion deterioration is overcompensated by the reduced heat exchange losses. The results do not indicate the presence of a peak. An extension of the present analysis, with the aim of testing λ > 2.9, might provide higher efficiency and additional details in cyclic variability. In addition, as well-known for SI gasoline engines, the combustion retard progressively reduces the brake efficiency due to the less favorable thermodynamic conditions of the mixture, resulting in slower flame propagation. It is worth noting that the progressive reduction in brake efficiency is more pronounced for leaner mixtures, thus indicating that the weight of the heat exchange losses is reduced compared to the deterioration of the combustion efficiency. In addition, retarding the combustion process leads to an increment of cyclic variability, and the leaner the mixture, the higher the variability, as shown in Fig. 10 (B). Therefore, although retarded combustion allows more time for the mixture homogenization [40], the CoV of IMEP increases due to the less favorable thermodynamic conditions within the cylinder during the combustion process. This result is also confirmed by the test presented in Fig. 6 (B), in which the EOI = −110 deg ATDCf case shows that the impact of mixture inhomogeneity is limited, thus leading to a low cyclic variability. As far as NO_X emissions are concerned, advanced combustion phasing leads to higher emissions due to faster combustion and higher in-cylinder temperature. The impact of combustion timing on the NO_X emissions can be highlighted for each λ tested; however, the richer condition (i.e., λ = 2.1) emphasizes it showing a remarkable NO_X reduction retarding the combustion. Nevertheless, looking at the other λ values, mixture enleanment is definitely more effective than retarding combustion for the control of NO_X emissions, ensuring high efficiency at the same time.

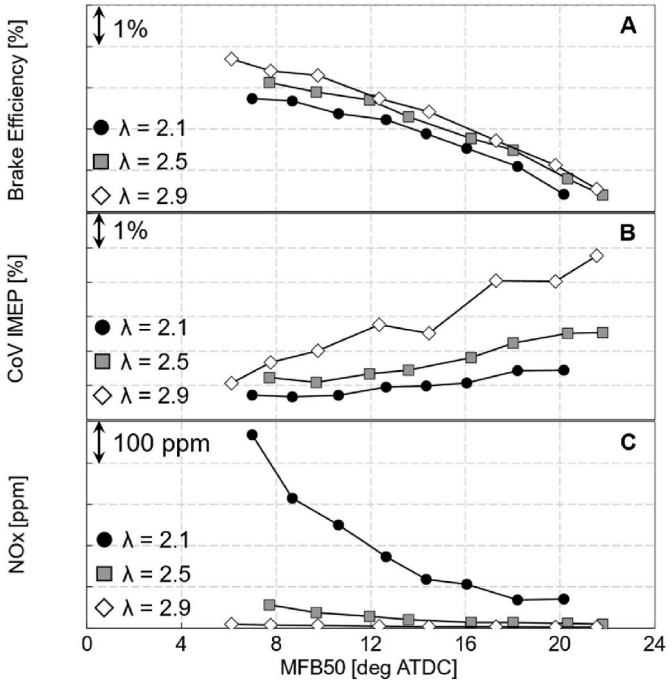

Fig. 10. Test#2 – MFB50 Sweep: effect of combustion timing under different λ conditions.
A: Brake efficiency. B: CoV IMEP. C: NO_X emissions.

In Fig. 11, the average in-cylinder pressure and the corresponding normalized burn rate are shown for the MFB50 sweep at λ = 2.5. As a consequence of the retarded combustion timing, the efficiency reduces, so the boost pressure increases in order to maintain the same load and λ. The burn rates exhibit a similar pattern, with an initial phase characterized by a rapid increase in burn rate, followed by a more gradual decrease in the second phase. Retarding the combustion timing results in a reduction of both the peak burn rate and the rate of burn rate growth. As anticipated, the impact on in-cylinder pressure is a shift in timing and a reduction in the pressure peak. Notably, for the most retarded combustion timing, the peak pressure presents a value comparable to that observed in the motored cycle.

The impact of the combustion phasing over different mixture compositions has been also analyzed considering the 200 individual cycles acquired in each engine operating condition under investigation. Therefore, Fig. 12 shows the maximum pressure for each cycle as a function of its crank angle for the three tested λ in order to add further insights on the lean limit, as evidenced by the works of Matekunas [34], and Granet [41]. In each plot, three combustion timings are reported, moving from an advanced one in red to a retarded one in green.

Starting from λ = 2.1 case in Fig. 12 (A), it is evident that the relationship between the maximum pressure and crank angle of maximum pressure is linear since the operating condition is far from the lean limit. In this case, retarding the combustion start moves the peak pressure ahead in the engine cycle, thus resulting in lower peak pressure. This plot provides further detail: the dispersion of the points at the same spark timing, indeed, can be considered as an indicator of combustion variability. Considering a certain value of the crank angle of maximum pressure, it is possible to identify the individual pressure cycle that shows the highest and the lowest peak pressure. Repeating this procedure to all crank angles, two lines can be identified: one corresponding to the highest value of the peak pressure, labeled “Fast Burn”, and one corresponding to the lowest value of the peak pressure, labeled “Slow Burn” in Fig. 12. The terms “fast” and “slow”, already used in Matekunas [34], are derived from the consideration that, for a specific crank angle of maximum pressure, the highest peak pressure is achieved by a cycle in which more fuel is burned from spark timing to the considered crank

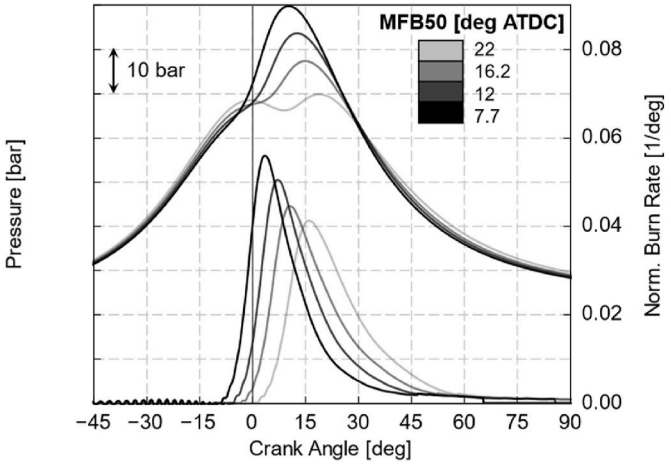

Fig. 11. Experimental in-cylinder pressure average cycles and normalized burn rate of a MFB50 sweep at λ = 2.5.

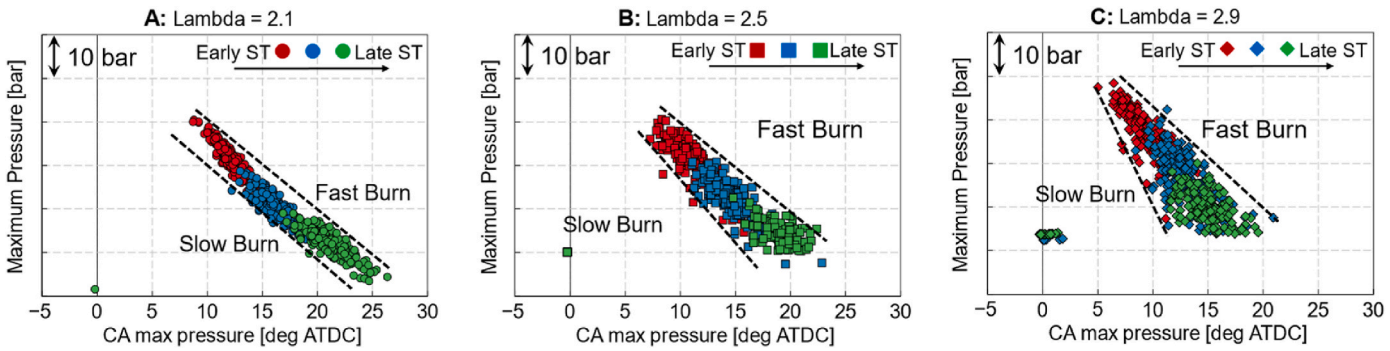

Fig. 12. Matekunas plots
A: λ = 2.1; B: λ = 2.5; C: λ = 2.9.

angle (fast cycle), while the lowest peak pressure is reached by cycle in which less fuel is burned (slow cycle). At λ = 2.1, a parallel trend between the "Fast Burn" and the "Slow Burn" lines can be highlighted, thus indicating that the cyclic variability of the three different combustion timings is similar. Considering the λ = 2.5 operating conditions in Fig. 12 (B), as the combustion timing is retarded, the dispersion of the points increases, resulting in a diverging trend between the "Fast Burn" and the "Slow Burn" lines. This confirms that combustion retardation leads to a significant increase in the combustion variability. The case at λ = 2.9 (Fig. 12 (C)) further confirms the above considerations. The dispersion is largely increased for the retarded combustion timings, and the fast and slow burn lines are no longer parallel. In addition, several points show a constant peak pressure value with a crank angle of maximum pressure close to TDC, thus exhibiting a slow combustion process.

In the end, this analysis has demonstrated that the exploitation of ultra-lean λ values is an effective solution to achieve high efficiency with acceptable combustion stability and reduced NO_X emissions when optimal combustion timings are adopted. However, the sensitivity to combustion phasing is enhanced compared to lower λ cases.

As abovementioned, in the Test #2 results, the maximum efficiency has been reached with λ = 2.9 and the most advanced combustion timing (MFB50 = 6 deg ATDCf), as shown in Fig. 10. To better understand this trend, Fig. 13 depicts the net indicated efficiency of each individual pressure cycle as a function of the MFB50, for each value of λ.

The cases with λ = 2.1 show generally lower efficiencies compared with leaner λ with a reduced dispersion along the trend line. The peak efficiency is reached for values of MFB50 between 5 and 10 deg ATDCf, with the value that remains almost constant within this crank angle window. Increasing λ up to λ = 2.5, the peak efficiency increases, and the sensitivity to the MFB50 becomes more pronounced than the λ = 2.1 case. The efficiency peak is close to MFB50 = 6 deg ATDCf, slightly advanced compared to the previous one. The case at λ = 2.9 exhibits the same behavior. The peak efficiency is higher, and it is reached with a combustion anchor angle more advanced than the other λ values. In particular, even considering the higher variability induced by the leaner mixture composition, in this case the maximum efficiency is achieved with a MFB50 = 4 deg ATDCf. It is worth noting that the loss of efficiency is particularly evident for retarded combustion timings, thus highlighting the fact that the leaner the mixture composition, the higher the sensitivity to the combustion phasing. The peak efficiency is defined as the condition at which the sum of the combustion of both duration loss and the heat exchange losses is minimized. For leaner λ values, the relative weight of the heat exchange losses is reduced, due to the lower peak temperatures reached in the combustion chamber. Another important factor is the increase of the quenching distance with leaner mixtures, due to the increment of the flame thickness, as demonstrated by Suckhart et al. [42]. On the other hand, the losses resulting from the leaner combustion process increase, due to the lower flame speed and

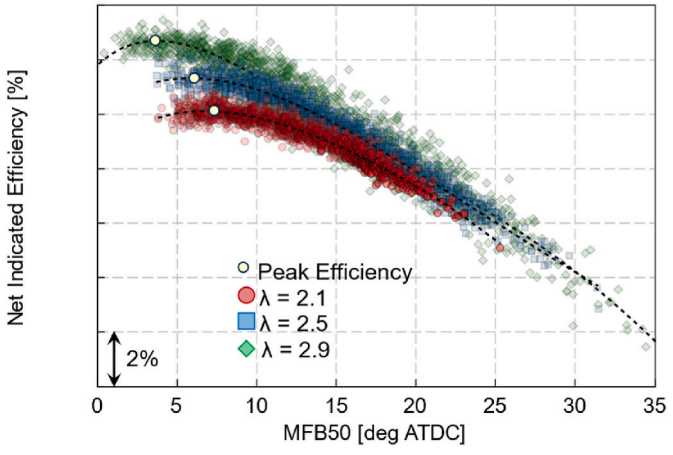

Fig. 13. Individual pressure cycle analysis: net indicated efficiency as a function of the MFB50 for three levels of λ

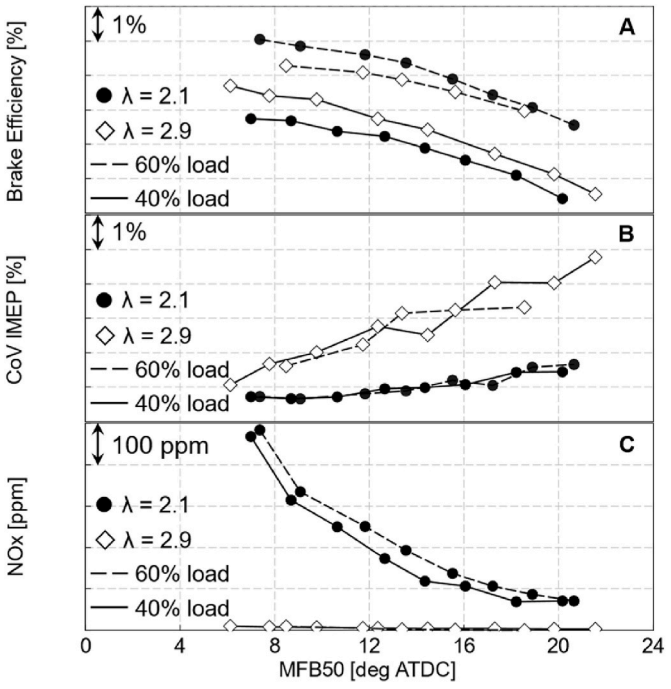

Fig. 14. Test#2 – MFB50 Sweep: effect of combustion timing under different load conditions.
A: Brake efficiency. B: CoV IMEP. C: NO_X emissions.

the increased unburnt fuel. The combination of these two factors resulted in an advancement of peak efficiency towards the TDC. On the contrary, at $\lambda = 2.1$, the relative weight of these two components is reversed. While combustion duration losses are less significant for the higher flame speed, heat exchange losses are more pronounced, due to the higher peak temperatures reached during the combustion and the shorter quenching distance. These findings are consistent with those reported by Fu et al. [43], which showed that in a spark timing sweep, brake thermal efficiency reached its peak in advance when the mixture was leaner.

In Fig. 14, a comparison with the results obtained at 60% of maximum load at 1100 rpm is shown. For the sake of brevity, only the cases at $\lambda = 2.1$ and $\lambda = 2.9$ are reported. Retarding the combustion timing provides a similar deterioration of brake efficiency. A different behavior is present regarding λ, as abovementioned in the discussion of Fig. 9 – (A). Also in these cases, the decrease in brake efficiency at $\lambda = 2.9$ is caused by the increased PMEP. As far as concern the combustion variability and NO_X emissions, the increase of load does not introduce significant variation in the results.

4. Conclusions

In this paper, a wide experimental analysis was carried out to investigate and understand the influence of the main engine calibration parameters on the performance and emissions of a 6-cylinder, 12.9-L, direct-injection spark-ignition hydrogen ICE, retrofitted from a PFI compressed NG one. With this aim, the impact of the relative air-fuel equivalence ratio, spark advance, and injection timing on the combustion and emissions formation phenomena was examined. The main remarks are summarized as follows:

1. Injection timing retard increases efficiency of around 1.5%, but, mainly for $\lambda = 2.9$ cases, the mixture results to be more inhomogeneous. The increase in combustion variability (+2% at $\lambda = 2.9$) and NO_X emissions (+200 ppm at $\lambda = 2.1$) limit the injection retard. Moreover, this study demonstrated that mixture inhomogeneity has a significant influence on the duration of the initial combustion phase (MFB0-10%), as evidenced by the increase in combustion variability.
2. The sweep of combustion timing has highlighted that the brake efficiency of lean mixtures is more influenced by the combustion retard. The highest efficiency was achieved at $\lambda = 2.9$ with the most advanced combustion timing. Even though a peak of efficiency seems not achieved, the exploration at higher λ values was not performed, since higher values of λ could result in limitations on the turbocharger side. In those conditions, both combustion variability and NO_X emissions (−80% compared to $\lambda = 2.1$ at the same MFB50) were kept under control.
3. A dependency between the MFB50 of peak efficiency and the λ was identified. As the mixture became leaner, the relative change of weight of heat exchange losses and combustion efficiency resulted in a more advanced MFB50 of peak efficiency. A difference of around 4 deg was observed between the MFB50 of peak efficiency at $\lambda = 2.1$ and the MFB50 of peak efficiency at $\lambda = 2.9$.

CRediT authorship contribution statement

Andrea Piano: Writing – review & editing, Supervision, Methodology, Conceptualization. **Francesco Pucillo:** Writing – original draft, Visualization, Methodology, Formal analysis. **Federico Millo:** Supervision, Project administration, Conceptualization. **Sergio Giordana:** Supervision, Project administration. **Nicola Rapetto:** Writing – review & editing, Supervision, Project administration, Conceptualization. **Christoph Schuette:** Visualization, Investigation, Data curation.

Declaration of competing interest

The authors declare that they have no known competing financial interests or personal relationships that could have appeared to influence the work reported in this paper.

Definitions/Abbreviations

ICE	Internal combustion engine
NO_X	Nitrogen oxides
PFI	Port fuel injection
NG	Natural gas
DI	Direct injection
PM	Particulate matter
MFB50	Crank angle at 50% of mass fraction burned
ATDCf	After top dead center firing
λ	Air-to-fuel relative equivalence factor
EOI	End of injection
CoV	Coefficient of variability
IMEP	Indicated mean effective pressure
SI	Spark ignition
MFB0-10%	Burn duration between 0 and 10% of mass fraction burned

References

[1] European Council, “Fit for 55”, https://www.consilium.europa.eu/en/policies/green-deal/fit-for-55-the-eu-plan-for-a-green-transition/, accessed on Jan. 2024.
[2] U.S. Congress, “H.R.5376-Inflation Reduction Act of 2022”, https://www.congress.gov/bill/117th-congress/house-bill/5376/text.
[3] ITF Transport Outlook. Decarbonising transport: scenarios for the future. https://www.oecd-ilibrary.org/sites/09f48ecd-en/index.html?itemId=/content/component/09f48ecd-en#section-d1e7667-adea820d82; 2023. accessed on May 2024.
[4] Onorati A, Payri R, Vaglieco BM, Agarwal AK, Bae C, Bruneaux G, et al. The role of hydrogen for future internal combustion engines. Int J Engine Res 2022;23(4):529–40. https://doi.org/10.1177/14680874221081947.
[5] U.S. Department of Energy, “U.S. National Clean Hydrogen Strategy and Roadmap”, https://www.hydrogen.energy.gov/library/roadmaps-vision/clean-hydrogen-strategy-roadmap, accessed on Jan. 2024.
[6] European Commission, EU “Hydrogen strategy” https://energy.ec.europa.eu/topics/energy-systems-integration/hydrogen_en, accessed on Jan. 2024.
[7] The Ministerial Council on Renewable Energy, Hydrogen and Related Issues, “Basic Hydrogen Strategy”, https://www.meti.go.jp/shingikai/enecho/shoene_shinene/suiso_seisaku/pdf/20230606_5.pdf, accessed on Jan. 2024.
[8] Gürbüz H, Akçay H, Demirtürk S, Topalcı Ü. Techno-enviro-economic comparison analysis of a PEMFC and a hydrogen-fueled SI engine. Appl Therm Eng 2024;243. https://doi.org/10.1016/j.applthermaleng.2024.122528.
[9] Maio G, Boberic A, Giarracca L, Aubagnac-Karkar D, Colin O, Duffour F, et al. Experimental and numerical investigation of a direct injection spark ignition

hydrogen engine for heavy-duty applications. Int J Hydrogen Energy 2022;47(67):29069–84. https://doi.org/10.1016/j.ijhydene.2022.06.184.
[10] Verhelst S, Wallner T. Hydrogen-fueled internal combustion engines. Prog Energy Combust Sci 2009;35(6):490–527. https://doi.org/10.1016/j.pecs.2009.08.001.
[11] Millo F, Piano A, Rolando L, Accurso F, Gullino F, Roggio S, et al. Synergetic application of zero-, one-, and three-dimensional computational fluid dynamics approaches for hydrogen-fuelled spark ignition engine simulation. SAE Int J Engines 2021;15(4). https://doi.org/10.4271/03-15-04-0030.
[12] Wallner T, Lohse-Busch H, Gurski S, Duoba M, Thiel W, Martin D, Korn T. Fuel economy and emissions evaluation of BMW Hydrogen 7 Mono-Fuel demonstration vehicles. Int J Hydrogen Energy 2008;33(24):7607–18. https://doi.org/10.1016/j.ijhydene.2008.08.067.
[13] Thomas Koch D, Sousa A, Bertram D. H2-Engine operation with EGR achieving high power and high efficiency emission-free combustion. 2019. https://doi.org/10.4271/2019-01-2178.
[14] Pauer T, Weller H, Schünemann E, Eichlseder H, Grabner P, Schaffer K. H2 ICE for future passenger cars and light commercial vehicles. Proceedings of the 41st international Vienna motor symposium. VDI Verlag; 2020. https://doi.org/10.51202/9783186813121. ISBN 9783186813121.
[15] Brauer M, Maaß J, Römer L Von, Riess M, Sens M, Tschiggfrei W, et al. Optimization of the mixture formation in DI hydrogen combustion engines by modified injector nozzle design. 31st aachen colloquium sustainable mobility. 2022. ISBN 9783000725241.
[16] Gao J, Wang X, Song P, Tian G, Ma C. Review of the backfire occurrences and control strategies for port hydrogen injection internal combustion engines. Fuel 2022;307. https://doi.org/10.1016/j.fuel.2021.121553.
[17] Dhyani V, Subramanian KA. Fundamental characterization of backfire in a hydrogen fuelled spark ignition engine using CFD and experiments. Int J Hydrogen Energy 2019;44(60):32254–70. https://doi.org/10.1016/j.ijhydene.2019.10.077.
[18] Dober G, Hoffmann G, Piock WF, et al. An efficient path to zero CO2 powertrains – BorgWarner's hydrogen injection systems. Proceedings of the 43rd international Vienna motor symposium 27 - 29 april 2022. 2022. ISBN 9783950496918.
[19] Matthias NS, Wallner T, Scarcelli R. A hydrogen direct injection engine concept that exceeds U.S. DOE light-duty efficiency targets. SAE Int J Engines 2012;5(3):838–49. https://doi.org/10.2307/26277511.
[20] Tsukamoto Y, Tanno S, Miyamoto Y, et al. Analysis of the effect of hydrogen combustion characteristics on engine performance. 2023.
[21] Poursadegh F, Brear M, Hayward B, Yang Y. Autoignition, knock, detonation and the octane rating of hydrogen. Fuel 2023;332. https://doi.org/10.1016/j.fuel.2022.126201.
[22] Thawko A, Tartakovsky L. The mechanism of particle formation in non-premixed hydrogen combustion in a direct-injection internal combustion engine. Fuel 2022;327. https://doi.org/10.1016/j.fuel.2022.125187.
[23] Grabner P, Schneider M, Gschiel K. Formation mechanisms and characterization of abnormal combustion phenomena of hydrogen engines. 2023. https://doi.org/10.4271/2023-32-0168.
[24] Schneider S, Trabold C, Friedrich T, Mayer F, Weller F, Stiehl R. H2 ICE DI multicylinder engine tests for thermodynamics and component development. Heavy-Duty-, On- und Off-Highway-Motoren 2022. Wiesbaden: Springer Vieweg; 2023. p. 40–52. https://doi.org/10.1007/978-3-658-41477-1_4. ISBN 978-3-658-41477-1.
[25] Maio G, Kumar R, Matthieu Andre L, Rouleau L, Walter B, Laget O, et al. Retrofitting a diesel baseline to a fully H 2 spark ignition engine by combining experiments, 0D/1D, and 3D CFD simulations. 31st Aachen Colloquium Sustainable Mobility, Paper n. 61, 2022. ISBN 978-3-00-072524-1.
[26] Berg V, Koopmans L, Sjöblom J, Dahlander P. Characterization of gaseous and particle emissions of a direct injection hydrogen engine at various operating conditions. SAE Technical Papers, SAE International 2023. https://doi.org/10.4271/2023-32-0042.
[27] Kufferath A, Naber D, Cornetti G, et al. Development of combustion process and operating strategy for a low-emission hydrogen engine. 31st aachen colloquium sustainable mobility. 2022. ISBN 9783000725241.
[28] Kunder N, Arnberger A, Araujo A, et al. Exhaust aftertreatment system development to achieve EURO 7 compliance with the heavy-duty AVL hydrogen engine. Lille, FR: presentation at SIA Powertrain 2024 - International Congress & Exhibition; 2024.
[29] Yeganeh M, Akram MS, Cheng Q, Karimkashi S, Kaario O, Larmi M. Experimental study of hydrogen jet dynamics: investigating free momentum and impingement phenomena. Int J Hydrogen Energy 2024;68:1423–37. https://doi.org/10.1016/j.ijhydene.2024.04.296.
[30] Dober G, Hoffmann G, Piock W, Doradoux L, Meissonnier G, et al. Application of H 2 ICE technology on commercial vehicles. 31st aachen colloquium sustainable mobility. 2022. ISBN 9783000725241.
[31] Scalambro A, Piano A, Millo F, Scinicariello N, et al. Numerical analysis of the hydrogen-air mixture formation process in a direct-injection engine for off-road applications. Int J Hydrogen Energy 2024;77:1286–95. https://doi.org/10.1016/j.ijhydene.2024.06.193.
[32] Lee S, Kim G, Bae C. Behavior of hydrogen hollow-cone spray depending on the ambient pressure. Int J Hydrogen Energy 2021;46(5):4538–54. https://doi.org/10.1016/j.ijhydene.2020.11.001.
[33] Li X, Sun B, Zhang D, Wang X, Bao L, Luo Q. Experimental study on the cycle variation characteristics of direct injection hydrogen engine. Energy Convers Manag X 2022;15. https://doi.org/10.1016/j.ecmx.2022.100260.
[34] Matekunas FA. Modes and measures of cyclic combustion variability. 1983.
[35] Heywood J. Internal combustion engine fundamentals. second ed. New York, NY, USA: McGraw Hill Professional; 2018.
[36] Laichter J, Kaiser SA, Rajasegar R, Srna A. Impact of mixture inhomogeneity and ignition location on early flame kernel evolution in a direct-injection hydrogen-fueled heavy-duty optical engine. 2023.
[37] Liang Z, Xie F, Lai K, Chen H, Du J, Li X. Study of single and split injection strategies on combustion and emissions of hydrogen DISI engine. Int J Hydrogen Energy 2024;49:1087–99. https://doi.org/10.1016/j.ijhydene.2023.10.060.
[38] Kim YY, Lee JT, Choi GH. An investigation on the causes of cycle variation in direct injection hydrogen fueled engines. Int J Hydrogen Energy 2005;30(1):69–76. https://doi.org/10.1016/j.ijhydene.2004.03.041.
[39] Pucillo F, Millo F, Piano A, Giordana S, Rapetto N, Paulicelli F. Turbocharging system selection for a hydrogen-fuelled spark-ignition internal combustion engine for heavy-duty applications. SAE Technical Papers, SAE International; 2024. https://doi.org/10.4271/2024-01-3019.
[40] Hamzehloo A, Aleiferis P. Numerical modelling of mixture formation and combustion in DISI hydrogen engines with various injection strategies. SAE Technical Papers, SAE International; 2014. https://doi.org/10.4271/2014-01-2577.
[41] Granet V, Vermorel O, Lacour C, Enaux B, Dugué V, Poinsot T. Large-Eddy Simulation and experimental study of cycle-to-cycle variations of stable and unstable operating points in a spark ignition engine. Combust Flame 2012;159(4):1562–75. https://doi.org/10.1016/j.combustflame.2011.11.018.
[42] Suckart D, Linse D, Schutting E, Eichlseder H. Experimental and simulative investigation of flame–wall interactions and quenching in spark-ignition engines. Automotive and Engine Technol 2017;2(1–4):25–38. https://doi.org/10.1007/s41104-016-0015-z.
[43] Fu Z, Li Y, Wu W, Li Y, Gao W. Experimental study on the combustion and emission performance of the hydrogen direct injection engine. Int J Hydrogen Energy 2024;61:1047–59. https://doi.org/10.1016/j.ijhydene.2024.02.276.